Number of text pages including figures and tables:33
Number of figures: 5
Number of tables: 0

**Article type:** Research Article

**Title:** Optical detection of neuron connectivity by random access two-photon microscopy

**Author:** Nasrin Shafeghat[1,*], Morteza Heidarinejad[1], Noboru Murata[2], Hideki Nakamura[1,**], and Takafumi Inoue[1]

[1]Department of Life Science and Medical Bioscience and [2]Department of Electrical Engineering and Bioscience, School of Advanced Science and Engineering, Waseda University, Tokyo, Japan

[*]present address: Laboratory for Neural Circuit Theory, Brain Science Institute, RIKEN, Wako, Saitama, Japan.

[**]present address: Department of Cell Biology, Johns Hopkins University, Baltimore, U.S.A.

**Corresponding Author:** Takafumi Inoue, M.D., Ph.D.
Department of Life Science and Medical Bioscience
Waseda University,
2-2 Wakamatsu-cho, Shinjuku,
Tokyo-162-8480, Japan
tel: +81-3-5369-7328
e-mail: inoue.t@waseda.jp

## Abstract

**Background:** Knowledge about the distribution, strength, and direction of synaptic connections within neuronal networks are crucial for understanding brain function. Electrophysiology using multiple electrodes provides a very high temporal resolution, but does not yield sufficient spatial information for resolving neuronal connection topology. Optical recording techniques using single-cell resolution have provided promise for providing spatial information. Although calcium imaging from hundreds of neurons has provided a novel view of the neural connections within the network, the kinetics of calcium responses are not fast enough to resolve each action potential event with high fidelity. Therefore, it is not possible to detect the direction of neuronal connections.

**New Method:** We took advantage of the fast kinetics and large dynamic range of the DiO/DPA combination of voltage sensitive dye and the fast scan speed of a custom-made random-access two-photon microscope to resolve each action potential event from multiple neurons in culture.

**Results:** Long-duration recording up to 100 minutes from cultured hippocampal neurons yielded sufficient numbers of spike events for analyzing synaptic connections. Cross-correlation analysis of neuron pairs clearly distinguished synaptically connected neuron pairs with the connection direction.

**Comparison with Existing Method:** The long duration recording of action potentials with voltage-sensitive dye utilized in the present study is much longer than in previous studies. Simultaneous optical voltage and calcium measurements revealed that voltage-sensitive dye is able to detect firing events more reliably than calcium indicators.

**Conclusions:** This novel method reveals a new view of the functional structure of neuronal networks.

## Keywords:

voltage sensitive dye, random access two-photon microscopy, population spike recording, neural connectivity

Abbreviations:

4AP: 4-aminopyridine
ACSF: artificial cerebrospinal fluid
AM: acetoxymethyl
AOD: acoust-optic deflector
Ca: calcium
$[Ca^{2+}]_i$: intracellular calcium concentration
DIV: days in vitro
DiO: dioctadecyl-3,3,3,3-tetramethylindocarbocyanine percholorate
DPA: dipicrylamine
DMSO: dimethyl sulfoxide
GEVI: genetically encoded voltage indicator
VSD: voltage sensitive dye

## 1. Introduction

Although many attempts have been made to determine the topology and direction of neuronal connections in neuronal networks by monitoring neuronal activities, satisfactory techniques have yet to be developed. There is a long history of electrophysiological techniques, which provide high temporal resolution with high fidelity. The multi-electrode array method allows for detection of activities of hundreds of neurons. However, it lacks the single-cell level resolution and capability for morphological identification of recorded neurons, which is why spike sorting is required for neuronal identification (Takahashi et al. 2003; Buzsáki 2004; Vigneron and Chen 2014). Conversely, optical methods provide high spatial resolution and identification of each neuron. Recording intracellular calcium ion ($Ca^{2+}$) concentration ($[Ca^{2+}]_i$) has become popular for investigating activities of neuron populations (Grienberger and Konnerth 2012) and has revealed neuronal connection maps (Stetter et al. 2012). However, $[Ca^{2+}]$ monitoring is an indirect measure of action potentials and, thus, cannot accurately follow voltage changes in each action potential. Additionally, the slow kinetics of $[Ca^{2+}]_i$ hinders the detection of each neuron connection direction.

Optical measurements of membrane potential with voltage-sensitive dyes (VSDs) are capable of sensing potential changes at a sub-millisecond order, and are promising in terms of spatial and temporal resolutions. VSDs have successfully enabled the recording of action potential events from a population of neurons in a single trial, without averaging, in invertebrate (Grinvald et al. 1977; Wu et al. 1994) and vertebrate peripheral nervous systems (Neunlist et al. 1999; Obaid et al. 1999). However, single trial spontaneous action potential recordings in the central nervous system have only recently been reported in single neurons (Pagès et al. 2011) and multiple neurons (Yan et al. 2012) *via* newly developed VSDs and advanced optical devices. This can be attributed to the relatively poor signal-to-noise ratio of the majority of VSDs compared to Ca indicators, and also to the slow frame rate of laser scanning microscopes required for fluorescence imaging.

Random-scanning two-photon microscopy provides high temporal and spatial resolution with flexibility in point selection, reduced total exposure light, reduced scattering

of laser light and the elimination of unnecessary fluorescence emission (Bullen and Saggau 1999; Salome et al. 2006; Katona et al. 2012). The acousto-optic deflector (AOD) adopted in microscopy helps attain a temporal resolution > 10 kHz. The AOD also allows access to any point of the field of view within microseconds. By adding a third AOD for z-axis adjustment, three dimensional random access is capable without reducing time resolution (Reddy and Saggau 2005; Katona et al. 2012). Recording spontaneous action potentials from multiple neurons was first made possible using random-access two-photon microscopy with a new generation of VSDs (Yan et al. 2012). However, a key feature necessary for neuronal network determination is still missing, i.e., long-duration recording. There has been no study showing stable action potential recording at single cell resolution for extended periods longer than 10 minutes using two-photon microscopy. No less than ten minutes of neuron activity recording is necessary to determine the neuron connections and connectivity direction or for monitoring mode transitions in connections of neuron networks using pharmacological interventions. Because excitatory interactions between neurons in the central nervous system are generally weak (Mason et al. 1991; Deuchars et al. 1994; Markram et al. 1997; Thomson and Deuchars 1997; Thomson et al. 2002), the accumulation of many spike events is needed (Schwindel et al. 2014).

In this study, the action potentials of multiple-cultured hippocampal neurons, a simple neuron network model system (Ivenshitz and Segal 2010; Sporns 2010), were recorded using the DiO/DPA VSD and an AOD-driven random scanning two-photon microscope. DiO/DPA is a VSD comprised of dioctadecyl-3,3,3,3-tetramethylindocarbocyanine percholorate (DiO) and dipicrylamine (DPA) with fast sub-millisecond kinetics and a large dynamic range (Chanda et al. 2005; Bradley et al. 2009; Fink et al. 2012). With this experimental setup, we succeeded in stably recording spike trains of multiple neurons for more than thirty minutes. Accumulated spike events enabled us to analyze neuron connections and the direction of connections between pairs of neurons in a robust manner.

## 2. Materials and Methods

### *2.1. Experimental animal and neuronal cultures*

Animal care was in accordance with guidelines outlined by the Institutional Animal Care and Use Committee of Waseda University. The protocol was approved by the Committee on the Ethics of Animal Experiments of Waseda University (2011-A068). Throughout all experimental procedures, efforts were made to minimize the number of animals used and their suffering. The primary culture from Wistar rat hippocampi was prepared according to a standard method (Bannai et al. 2009). Primary cultured neurons at 9–24 days *in vitro* (DIV) were used.

### *2.2. Electrophysiology*

Artificial cerebrospinal fluid (ACSF) consisting of (in mM) 124 NaCl, 2.5 KCl, 2 $CaCl_2$, 2 $MgCl_2$, 1.25 $NaH_2PO_4$, 26 $NaHCO_3$, and 20 glucose bubbled with a mixture of 95% $O_2$ and 5% $CO_2$ was superfused throughout experiments. The temperature was maintained at 29–35ºC. For patch-clamp recording glass pipettes of 5 MΩ, tip resistance was pulled from borosilicate glass capillaries (Sutter Instrument, Navato, CA, USA), which were filled with an internal solution consisting of (in mM): 130 K gluconate, 5 KCl, 5 NaCl, 10 HEPES, 0.4 EGTA, 1 $MgCl_2$, 4 $Na_2ATP$, and 4 NaGTP (pH 7.25, 300 mOSm). Cells were identified using differential interference contrast (DIC) optics and a charge-coupled device camera (CFW-1612M, Scion Corp, Frederick, MD, USA). Patch-clamp recordings were performed using a Multiclamp 700B amplifier (Molecular Device, Sunnyvale, CA, USA). Analogue signals were filtered at 10 kHz using a built-in low-pass Bessel filter in the amplifier and fed into an interface device (ITC-18, HEKA Elektronik, Lambrecht, Germany). The membrane potential was maintained at -60 mV in either the voltage- or current- clamp mode.

### *2.3. Optical configuration*

A custom-made two-photon scanning microscope was used to monitor fluorescence of VSD and calcium indicators equipped with a femtosecond pulsed Ti:Sapphire laser ( $\lambda$ = 930 nm, average output = 500–700 mW, Tsunami, Spectra Physics Japan, Tokyo, Japan)

pumped by a green laser ( $\lambda$ = 532 nm, 7.5 mW, Millenia, Spectra Physics Japan). An upright microscope (BX51WI, Olympus, Tokyo, Japan) was used in combination with laser optics. A 20x water immersion lens (numerical aperture = 1.0, XLUMPlan FL, Olympus) was used. Laser spot radius was 0.35 μm on the target using this objective lens. In-house TI Workbench software, written by T.I. and running on a Mac computer (Mac Pro, Apple, Cupertino, CA, USA), controlled all devices and recorded electrophysiological and optical data.

We adopted the optical design of the AOD-driven scanning system developed by the L. Bourdieu group (Salome et al. 2006). For the overall settings, refer to Figure 1 of Salome et al. (2006) with the following details. The laser beam was deflected by two orthogonal AODs (DTSXY-400-850.950, AA Opto-Electronic, Orsay, France) to scan the view field. To compensate for spatial distortions, an acousto-optic modulator (AOM, MTS144-B47A15-720.950, AA Opto-Electronic) was inserted in the light path at a 45˚ with respect to the AOD axes. The large temporal distortion introduced by the AODs and AOM was compensated with negative chirp optics consisting of a double pass within two Brewster prisms. Using these optics, the laser pulse width was satisfactorily compensated: 100 fs at the exit of the objective lens was slightly broadened from the Tsunami laser exit (84 fs). The access time of each AOD was 11.5 μs, which was required to change deflection. Fluorescence was split by a dichroic mirror, splitting at 580 nm, and detected with two photomultiplier tubes (PMTs, H7422PA-40, Hamamatsu Photonics, Hamamatsu, Japan) after passing through the 500–550 nm band-pass filter or the long-pass 580-nm filter. The PMTs were operated in the photon-counting mode. PMT outputs were fed into a time-correlated single photon counting (TCSPC) module (SPC-150, Becker & Hickl GmbH, Berlin, Germany, (Becker 2013)).

### *2.4. Reagents for stimulation*

The $Mg^{2+}$-free ACSF solution removal of $Mg^{2+}$ was compensated with an increased concentration of $CaCl_2$. Picrotoxin and 4-aminopyridine (4AP) were purchased from Indofine Chemical Co., Hillsborough, NJ, USA and Wako Pure Chemical Industries Ltd., Tokyo, Japan, respectively. High $K^+$ACSF solutions were prepared with different $[K^+]$.

[$Na^+$] was reduced to compensate for the increased [$K^+$] to maintain a constant osmolality.

### *2.5. VSD and Ca indicator staining*

Cells were first stained with DiO using the gene-gun method (Helios, Bio-Rad, Hercules, CA, USA) (Gan et al. 2000; O'Brien and Lummis 2006). Gold particles of 1 μm diameter were used. To avoid large clusters of particles and also to protect cells from gas pressure, a polycarbonate isopore membrane filter of 3 μm pore size and $8 \times 10^5$ pore/$cm^2$ density (TSTP04700, Millipore, Tokyo, Japan) was inserted to the gene gun muzzle (Kettunen et al. 2002). DPA loading followed the DiO staining. DPA was loaded by bath application (2 μM) for 20 min followed by DPA superfusion (0.5 μM). Stock solution of DPA (Tokyo Chemical Industry, Tokyo, Japan and Biotium Corp., Hayward, CA, USA) was prepared as 20 mM stock in dimethyl sulfoxide (DMSO, Sigma-Aldrich, Tokyo, Japan) and its time at room temperature did not exceed 2 months. The 2 and 0.5 μM DPA working solutions were freshly prepared by diluting in the extracellular solution. In the case of double staining with the Ca indicator and VSD, the cells were loaded with a Ca indicator by incubating in an acetoxymethyl (AM)-ester solution after staining with DiO, followed by DPA staining by superfusion. Asante Calcium Red (AM) (TEFLabs, Austin, TX, USA) (Hyrc et al. 2013) or Fura Red AM (Life Technologies Japan, Tokyo, Japan) (Kurebayashi et al. 1993) was used as a Ca indicator. Temperature of the superfusing extracellular solution was kept within 29–32°C.

### *2.6. Peak detection method*

We adopted a template matching method (Segev et al. 2004; Prentice et al. 2011) for peak detection of spike events recorded with VSD. Action potentials in the VSD traces were convolved with an 86-msec width template, which was obtained by averaging 46 spike events recorded with VSD taken from a neuron (shown in Fig. 3). The timing of action potential peaks of the averaged VSD traces were adjusted by simultaneously recorded action potential peaks *via* electrophysiology. Entire VSD traces without noise reduction filters were scanned using this template, and a correlation coefficient was calculated for each time point. Along the duration of this correlation coefficient, positive

amplitude peaks > 0.3 and a duration longer than 2.5 ms were considered to reflect action potential events.

We also tested the Schmitt trigger peak detection method, which yielded similar results as the template matching method in a previous report (Grewe et al. 2010). However, this method required pre-filtering the raw VSD traces with a low-pass filter, which reduced temporal resolution. Thus, the template matching method was adopted as the peak detection method in this study. A time series of the spike event number was created from detected peak timing by binning with a 2-ms time window or bin ($X_i$, i = 1, .., $T$) for each neuron $X$, where T is the total number of bins throughout the observation.

### *2.7. Synaptic connection detection analysis of spike trains*

To analyze synaptic connection and direction,, a cross-correlation of spike timing ($X_i$ and $Y_i$, i = 1, .., $T$) was calculated for every neuron pair $X$ and $Y$. Whether two time series of spike timing of a neuron pair with a lag ( $\tau$ [bins]), $X_i$ and $Y_{i+\tau}$, have a correlation was tested under the null hypothesis that $X_i$ and $Y_{i+\tau}$ have no correlation. The statistic, $Q\tau = \frac{1}{T-\tau}\sum_{i=1}^{T-\tau} X_i Y_{i+\tau}$, will have normal distribution if $X_i$ and $Y_{i+\tau}$ have no correlation and $T$ is large enough. Thus, the test statistic, $Z = \frac{\hat{Q}_\tau - E[Q_\tau]}{\sqrt{V[Q_\tau]}}$, will have standard normal distribution with the null hypothesis, where $E[Q_\tau] = E[X]E[Y]$ and $V[Q_\tau] = \frac{1}{T-\tau}(E[X^2]E[Y^2] - E[X]^2E[Y]^2)$. Cross-correlograms were created with a time range of ±30 ms (Fig. 5C). We used the statistical method to judge if there was a correlation between each pair of spike events in each bin time. For analysis on the direction of synaptic connection, we excluded uncorrelated spike pairs (shown as gray bars in Fig. 5C), and neuron pairs sharing spike pairs < six were discarded. The direction of the synaptic connection was assessed using asymmetry of synaptic connection to the lag $\tau = 0$: the number of events in both sides of the cross-correlogram were compared using the chi-square test.

### *2.8. Software*

All offline analyses were performed using the TI Workbench, in-house software

written by T.I. running on a Mac computer in combination with Microsoft Excel (Microsoft Japan, Tokyo, Japan), and Igor Pro (Wavemetrics, Lake Oswego, OR, USA). Data are indicated as mean ± SEM.

## 3. Results

### *3.1. Electro-optical recording of membrane potential in primary cultured neurons*

To verify whether our system is capable of following action potentials, cultured neurons from rat hippocampus were stained with DiO using the gene gun method (Fig. 1A) (Gan et al. 2000; O'Brien and Lummis 2006; Kettunen et al. 2002). The cells were then stained with DPA (2 μM) by bath application. Bath application of DiO dissolved in methanol or DMSO resulted in denser intracellular staining than the gene gun method using endocytosed dye molecules, which reduced the voltage signal from the dye molecule in the plasma membrane (data not shown). Labeled cells were patch-clamped and maintained at -70 mV in the current-clamp mode, and a rectangular depolarization current was applied to evoke action potentials. Optical and electrical recordings were simultaneously performed. Timing of action potentials were faithfully reported by the DiO/DPA VSD from locations on the patch-clamped cell, while fluorescence recorded from locations that were not on the patch-clamed cell showed flat traces, indicating reliability of both temporal and spatial resolutions in our system (Fig. 1B). The change in fluorescence intensity ($\Delta F/F_0$) during action potentials ranged 25–30% with a 6.8 ± 1.1 SNR, which was in accordance with previous reports using DiO/DPA with either single-photon (24% with average SNR of 3~7 in cultured hippocampal neurons (Bradley et al. 2009)) or two-photon excitation (18% in neocortical pyramidal neurons in brain slices (Fink et al. 2012)). This signal strength was also equivalent with results using hemicyanine dyes and two-photon excitation (10–20% with a SNR of 10–30 (Yan et al. 2012)).

### *3.2. Long-period action potential recording using DiO/DPA*

Although VSDs involving DPA are one of the most successful classes of VSD, DPA is also known to distort and prevent action potentials by increasing capacitive load (Fernández et al. 1983; Chanda et al. 2005; DiFranco et al. 2007). We actually found that the kinetics of rising and falling phases of action potentials evoked by depolarizing pulses were slowed and the peak height was decreased by DPA exposure in a time-dependent manner (Figs. 2A and B) (Fernández et al. 1983). Previous studies using DiO/DPA reported evoked action

potential (Bradley et al. 2009; Fink et al. 2012), but long-period recordings of spontaneous spiking events with DiO/DPA has not been reported. Therefore, to evaluate the effects of DPA on induced neuronal activities over a longer time scale, we further examined the effects in the context of bursting activity of cultured neurons with various inducers of neuron firing (Fig. 2C). 4AP (100 μM), which induces neuron firing by blocking A-type K channels (Pongs 1999), evoked spike bursts in a neuron in the current-clamp mode (Fig. $2C_1$). Spiking was gradually inhibited 8 minutes after 2 μM DPA was added to the superfusing solution containing 4AP (Fig. $2C_2$) and ceased completely 16 min after addition of DPA (Fig. $2C_3$). The DPA inhibition effect was washed out within 2 minutes with ACSF containing 4AP (Fig. $2C_4$). After testing the blocking effect of DPA in various stimulating conditions, including picrotoxin (7 μM) (Gibbs et al. 1997), $Mg^{2+}$-free (Gibbs et al. 1997), high $K^+$ (3.8 and 5.5 mM) (Tancredi and Avoli 1987), and 4AP (50 and 100 μM), we chose 100 μM 4AP as a spiking induction solution in the following long-duration recordings, because of the longer lasting effect under DPA and shorter period for washout of the DPA inhibition effect compared to other reagents (Fig. 2D). In short period recordings, 50 μM 4AP was also used.

### *3.3. Simultaneous electro-optical recording of action potentials in a spontaneous firing neuron*

Membrane potential changes of cultured neurons were simultaneously recorded using optical and electrophysiological methods in the presence of 50 μM 4AP. Fluorescence changes of DiO/DPA were recorded from a single location (Fig. 3A, red cross), which showed each single spike event (Fig. 3B, upper trace, $\Delta F/F_0 = 17.5 \pm 2.5\%$ per 60 mV) in accordance with spikes recorded using the electrophysiological method (Fig. 3B). The half-width of action potentials reported with DiO/DPA was similar to electrophysiology results (8.4 and 8.6 msec, respectively, after averaging 46 unfiltered raw traces, Fig. 3D). This result shows that the optical measurement with DiO/DPA was faithful enough to detect single spike events with a sufficiently high temporal resolution.

### *3.4. Simultaneous Ca and VSD recording from multiple neurons*

Ca recording methods have often been used to detect excitation patterns of neuronal populations (Grienberger and Konnerth 2012). To evaluate the effectiveness of membrane potential recording compared with Ca recording, we directly compared the DiO/DPA voltage recording method with Ca recording methods. Red Ca indicators, Asante Calcium Red (Hyrc et al. 2013) or Fura Red (Kurebayashi et al. 1993), were used together with DiO/DPA, which emits green fluorescence. Generally, the Ca indicator was able to faithfully detect spike events (Fig. 4A lower panel), but sometimes failed to follow action potentials, especially in relatively high-frequency spiking events (Fig 4B lower panels). DiO/DPA recording, in contrast, seemed to detect single spikes in both low-frequency firing (Fig. 4A upper panel) and high-frequency spiking (Fig. 4B 2-3). The difference in spike detection sensitivity may reflect different operation modes of Ca channels and slow kinetics of $[Ca^{2+}]_i$ from the membrane potential. High-frequency spiking piles up the baseline $[Ca^{2+}]_i$, which hides each Ca transient that accompanies the action potentials (Fig. 4B3 and Grewe et al. 2010). Neuronal activation not only evokes action potentials, but also induces Ca waves and sparks driven by intracellular Ca release channels (Ross 2012) and Ca influx by opening Ca-permeable plasma membrane channels, *e.g.*, transient receptor potential (Trp) channels (Vennekens et al. 2012). Spike detection with Ca indicators must segregate spike events from the background dynamic Ca changes. Furthermore, numerous mechanisms regulate activities of voltage-gated Ca channels (Simms and Zamponi 2014), thus the amplitudes and kinetics of Ca transients that accompany the action potentials are also affected by them. Neurons express different types of voltage-gated Ca channels with different expression levels. Some neuronal populations may not express sufficient Ca channels to show Ca transients on action potentials. We observed many neurons with action potentials using the DiO/DPA system, but did not detect accompanying Ca transients using the Ca indicators (data not shown). This observation indicates that optical voltage measurement is more advantageous than Ca measurements in spike detection with even fidelity over neurons of various status and cell types.

### *3.5. Spike detection and synaptic connections*

Action potential events were detected by matching with a spike template waveform, which was constructed from VSD recordings in a neuron (see Materials and Methods and Fig. 3D). Spike events evoked with 100 μM 4AP were accumulated from 4–11 neurons in different experiments (Fig. 5A and B). Synaptic connections between spiking neuron pairs were investigated by calculating the cross-correlation of spike timing between each neuron pair using the asymmetry of the cross-correlogram (Fig. 5C). The asymmetry in the neuron pair 1-6 in Fig. 5C, for example, indicates that the direction of synaptic connection was from neuron 1 to 6. In pairs 2-3 and 4-6 in the same figure, directions were from neuron 2 to 3 and from 4 to 6, respectively. Pairs 1-2, 1-3, and 1-4 show symmetric cross-correlogram, suggesting that these neuron pairs share common presynaptic neurons or have reciprocal connections. The asymmetry in the cross-correlogram was statistically evaluated using the chi-square method (See Materials and Methods).

Ninety three out of 151 analyzed neuron pairs from 27 experiments shared more than five spike events within the time window (±30 ms). Out of the 93 neuron pairs, 57 showed asymmetric cross-correlation, *i.e*., unidirectional connections. The remaining 36 neuron pairs showed symmetric temporal orders of firing. The lag for each neuron pair was calculated by fitting the cross-correlograms to a Gaussian distribution (Fig. 5D).

## 4. Discussion

Optical mapping by multisite recording of the membrane potential is essential for investigating a neuronal network. Wide-field microscopy with a photodiode array or high-speed CCD cameras provides sufficient frequency to resolve action potentials with voltage sensitive dyes, while signals coming from out-of focus depths hamper the signal-to-noise ratio. Additionally, photodynamic damage and photobleach, due to strong illuminations, cause problems for long-period single-cell level recording. Single-photon confocal microscopy provides a better signal-to-noise ratio by removing the out-of-focus signal, but it cannot reach deep inside the tissue. Two-photon microscopy is, thus, the best choice for scanning neuronal network activities in slice or whole brain preparations; this method has minimal photodynamic damage due to the inherent optical properties (Homma et al. 2009; Grienberger and Konnerth 2012). However, the mechanical galvano mirror motion limits the frame rate of conventional two-photon microscopes to 30 Hz at most, which is not capable of monitoring spike events with VSDs from multiple locations scattered over a large spatial range. In the current study, we solved this drawback by adopting AOD-driven laser scanning, which enabled random-access two-photon microscopy (Bullen and Saggau 1999; Salome et al. 2006; Katona et al. 2012) with high spatial and temporal resolutions. The minimal photobleach gained by the point-to-point random scanning enabled stable, long-duration recordings for up to 100 minutes, which was ideal for analyzing neuronal connections to accumulate sufficient spike events. This long-duration recording also makes it possible to monitor gradual mode transitions in neuron network connection patterns using pharmacological interventions.

### *4.1. Gene gun provided high-density staining*

Highly lipophilic VSDs are difficult to load into neural preparations, which was the case for DiO. Bath application of VSDs was used to record population activity in neuronal circuits in cortical slices, but the resolution was not sufficient for single-cell levels (Yoshimura et al. 2005). The gene gun labeling method overcomes this technical difficulty, providing fast staining of multiple neurons without pipette manipulation (Grutzendler et al.

2003; O'Brien and Lummis 2006; Aseyev et al. 2013). We were successful in labeling multiple neurons in culture preparation in this study. With regard to the Aseyev *et al.* report about staining and recording action potentials from neurons in brain slice preparations with hemicyanine VSDs (Aseyev et al. 2013), population recordings from multiple neurons using random-scan two-photon microscopy may be applicable for brain slices or even in brains of living animals with the gene gun method.

### *4.2. DiO/DPA*

In this study, we adopted the DiO/DPA combination as a VSD, due to the high signal-to-noise ratio and high temporal resolution previously described (Bradley et al. 2009). The inhibitory and deforming effects of DPA to action potential generation observed in this study were attributed to increased membrane capacitance (Sjulson and Miesenböck 2008; Bradley et al. 2009). Additionally, DPA antagonizes NMDA-type glutamate receptors in a voltage-dependent manner (Linsenbardt et al. 2013), and DiO prolongs action potential kinetics (Fink et al. 2012). DPA concentrations should be optimized to minimize the blocking effect on action potential generation (Bradley et al. 2009). In this study, to obtain long-term stable recording without inhibition of action potential generation, cells were first saturated for 20 min with 2 μM DPA, followed by 0.5 μM DPA and 100 μM 4AP, which provided sustained firing of culture neurons for 99 ± 8 min.

Despite the inhibitory effect of DPA, the highly lipophilic property of DiO is beneficial for stable, long-duration recording: the lipophilic nature creates difficulties for dye loading, although the dye remains stable in the plasma membrane for hours and days (Honig and Hume 1989). Additionally, non-fluorescent DPA is less hydrophobic and can be loaded and washed from the plasma membrane by superfusion. The characteristics of the two DiO/DPA components enable one to adjust the DPA concentration in the plasma membrane, which is necessary to maintain the DPA concentration within a range that does not inhibit action potential generation, but effectively reports potential changes with a stable fluorescence intensity.

### *4.3. Perspective of VSD and Ca recording*

Because of the limited temporal resolution of commonly used Ca indicators with regard to spike timing, various VSDs have been developed in recent years. Among them, hemicyanine VSDs show a rapid response and a dynamic range that is large enough to report spontaneous single-spike events from cerebellar Purkinje cells in slices uisng a random-scan two-photon microscope (Yan et al. 2012). Although the important properties of a dye series for long-duration recording, such as photobleach and photodynamic toxicity, remain poorly understood, this type of VSD holds promise as a candidate for chemical VSD for multisite neuron network activity monitoring.

Genetically encoded voltage indicators (GEVIs) are another perspective in terms of cell selectivity and totally different dye-loading methods (Knöpfel 2012). The kinetics of early GEVI generations were too slow for action potential detection from single cells. However, recent efforts have succeeded in producing fast GEVIs. QuasAr GEVIs have even greater dynamic ranges than small molecule synthetic VSDs and enough stability to permit thirty minutes of recording (Hochbaum et al. 2014). QuasAr GEVIs require longer excitation wave lengths (> 1000 nm) than the wave length range covered by a conventional two-photon laser source. The excitation wave length mismatch and very weak fluorescence intensity still hinders QuasArs from being used in two-photon microscopy. In a recent report, however, QuasAr-based fluorescent protein-conjugated FRET VSDs overcame the wavelength mismatch and brightness issues, but with some sacrifice in kinetics and dynamic range of QuasArs (Gong et al. 2014). Efforts for improving GEVIs will produce more effective VSDs for neuron population recording at the single cell level.

Although Ca indicators enabled simultaneously monitoring of thousands of neurons, the dynamics were slower than the neural firing kinetics, which may hinder precise prediction of connection and direction between neurons. However, $[Ca^{2+}]_i$ reflects intracellular changes in neurons and could reveal important parameters in excited and silent neuronal modes. Simultaneous voltage and calcium recordings enhances our understanding of neuronal physiology by correlating membrane potential changes with intracellular events (Vogt et al. 2011; Storace et al. 2015).

### *4.4. Neural connections and directions*

Interdependency between two time series of neuron spikes can be estimated using a cross-correlation analysis (Perkel et al. 1967; Csicsvari et al. 1998; Schwindel et al. 2014). The peak in the cross-correlogram represents the connection pattern: the deviation from a zero time lag indicates the connection direction. To statistically judge the spike cross-correlation timing between a pair of neurons, the synchronization index (SI) is a useful index (Wiegner and Wierzbicka 1987). However, this method requires a relatively high frequency of events, which does not always occur. Therefore, we adopted another method to statistically evaluate neuron connections applicable to neuron groups with a lower spike frequency. In this method, each time lag ( $\tau$ ) was tested in the correlation of time series ($X_i$ and $Y_{i+\tau}$) in each neuron pair. As a result, we found that most $\tau$s in the VSD recording were correlated using this test (corresponding to the fact that most bars were colored black in Fig. 5C). After this filtering operation, the cross-correlograms showed apparent shifts in many of the neuron pairs, indicating that these neuron pairs have directional synaptic connections. Although the asymmetric and symmetric distributions of cross-correlograms were rather apparent in the histograms (Fig. 5), we used the chi-square test to quantify neuron pairs with synaptic connection directions. We focused on excitatory connections to show robustness of the recording method. In the future, inhibitory synaptic connections will be included in spike timing analysis.

### *4.5. Conclusion*

Synchronized spikes among a neural ensemble represent a higher order of complex dynamics in neuronal activities. It is postulated that correlated synaptic inputs from multiple common presynaptic neurons cause post-synaptic spike synchronization (Song et al. 2005; Yoshimura et al. 2005; Kampa et al. 2006; Otsuka and Kawaguchi 2008; Kazama and Wilson 2009; Sporns 2010; Takahashi et al. 2010). Investigations based on the functional topological aspect of connections of synchronous neurons or on the anatomical basis of synaptic connections have been performed, but still little is known about the mapping of large-scale synchronized neurons. In the current study, we developed a novel

experimental and analytical paradigm to detect both the presence and direction of neuronal connections in group of neurons ranging over > 100 μm. Experimentally, we took advantage of the high temporal resolution of DiO/DPA VSD, as well as the high-speed scanning property of a custom-made AOD-driven random-scanning two-photon microscope. We adopted a template matching method for the precise detection of the spike timing, and developed a method to statistically evaluate if arbitrary pairs of spikes in distinct neurons are correlated. By statistically examining the asymmetry of the resultant cross-correlogram for each neuron pair, we succeeded in estimating the existence and direction of synaptic connections between the neuron pair. The combination of fast and high-dynamic range VSDs, as well as random-scan two-photon microscopy, allowed for long periods of stable recordings, which will be a powerful tool for optical mapping of synaptic correlations and the direction of connections.

## 5. Acknowledgements

This work was supported by a Project for Private Universities: matching fund subsidy from MEXT (Ministry of Education, Culture, Sports, Science and Technology) of Japan (T.I.), JSPS KAKENHI Grant Numbers 22650066, 23113515, 23300121, and 26640016 (T.I.), and Grants for Excellent Graduate Schools (Practical Chemical Wisdom, MEXT of Japan, N.S.). The authors thank Drs. Manabu Tanifuji, Hiroyoshi Miyakawa, and Tomoki Fukai for valuable discussions, and Dr. Takeyuki Sugawara for technical advices on the gene gun method, and all the members of the Inoue Laboratory for fruitful discussions and technical assistance.

## 6. References


Aseyev N, Roshchin M, Ierusalimsky VN, Balaban PM, Nikitin ES. Biolistic delivery of voltage-sensitive dyes for fast recording of membrane potential changes in individual neurons in rat brain slices. J Neurosci Methods. 2013;212:17–27.

Bannai H, Lévi S, Schweizer C, Inoue T, Launey T, Racine V, et al. Activity-dependent tuning of inhibitory neurotransmission based on $GABA_AR$ diffusion dynamics. Neuron. 2009;62:670–82.

Becker W. TCSPC Handbook, 5th edition. Becker and Hickl GmbH; 2013.

Bradley J, Luo R, Otis TS, DiGregorio DA. Submillisecond optical reporting of membrane potential *in situ* using a neuronal tracer dye. J Neurosci. 2009;29:9197–209.

Bullen A, Saggau P. High-speed, random-access fluorescence microscopy: II. Fast quantitative measurements with voltage-sensitive dyes. Biophys J. 1999;76:2272–87.

Buzsáki G. Large-scale recording of neuronal ensembles. Nat Neurosci. 2004;7:446–51.

Chanda B, Blunck R, Faria LC, Schweizer FE, Mody I, Bezanilla F. A hybrid approach to measuring electrical activity in genetically specified neurons. Nat Neurosci. 2005;8:1619–26.

Csicsvari J, Hirase H, Czurko A, Buzsáki G. Reliability and state dependence of pyramidal cell-interneuron synapses in the hippocampus: an ensemble approach in the behaving rat. Neuron. 1998;21:179–89.

Deuchars J, West DC, Thomson AM. Relationships between morphology and physiology of pyramid-pyramid single axon connections in rat neocortex *in vitro*. J Physiol. 1994;478:423–35.

DiFranco M, Capote J, Quinonez M, Vergara JL. Voltage-dependent dynamic FRET signals from the transverse tubules in mammalian skeletal muscle fibers. J Gen Physiol. 2007;130:581–600.

Fernández JM, Taylor RE, Bezanilla F. Induced capacitance in the squid giant axon. Lipophilic ion displacement currents. J Gen Physiol. 1983;82:331–46.

Fink AE, Bender KJ, Trussell LO, Otis TS, DiGregorio DA. Two-photon compatibility and single-voxel, single-trial detection of subthreshold neuronal activity by a two-component optical voltage sensor. PLoS One. 2012;7:e41434.

Gan WB, Grutzendler J, Wong WT, Wong RO, Lichtman JW. Multicolor "DiOlistic" labeling of the nervous system using lipophilic dye combinations. Neuron. 2000;27:219–25.

Gibbs JW, Sombati S, DeLorenzo RJ, Coulter DA. Physiological and pharmacological alterations in postsynaptic $GABA_A$ receptor function in a hippocampal culture

model of chronic spontaneous seizures. J Neurophysiol. 1997;77:2139–52.

Gong Y, Wagner MJ, Zhong Li J, Schnitzer MJ. Imaging neural spiking in brain tissue using FRET-opsin protein voltage sensors. Nat Commun. 2014;5:3674.

Grewe BF, Langer D, Kasper H, Kampa BM, Helmchen F. High-speed in vivo calcium imaging reveals neuronal network activity with near-millisecond precision. Nat Methods. 2010;7:399–405.

Grienberger C, Konnerth A. Imaging calcium in neurons. Neuron. 2012;73:862–85.

Grinvald A, Salzberg BM, Cohen LB. Simultaneous recording from several neurones in an invertebrate central nervous system. Nature. 1977;268:140–2.

Grutzendler J, Tsai J, Gan W-B. Rapid labeling of neuronal populations by ballistic delivery of fluorescent dyes. Methods. 2003;30:79–85.

Hochbaum DR, Zhao Y, Farhi SL, Klapoetke N, Werley CA, Kapoor V, et al. All-optical electrophysiology in mammalian neurons using engineered microbial rhodopsins. Nat Methods. 2014;11:825–33.

Homma R, Baker BJ, Jin L, Garaschuk O, Konnerth A, Cohen LB, et al. Wide-field and two-photon imaging of brain activity with voltage- and calcium-sensitive dyes. Methods Mol Biol. 2009;489:43–79.

Honig MG, Hume RI. Dil and DiO: versatile fluorescent dyes for neuronal labelling and pathway tracing. Trends Neurosci. 1989;12:333–41.

Hyrc KL, Minta A, Escamilla PR, Chan PPL, Meshik XA, Goldberg MP. Synthesis and properties of Asante Calcium Red--a novel family of long excitation wavelength calcium indicators. Cell Calcium. 2013;54:320–33.

Ivenshitz M, Segal M. Neuronal density determines network connectivity and spontaneous activity in cultured hippocampus. J Neurophysiol. 2010;104:1052–60.

Kampa BM, Letzkus JJ, Stuart GJ. Cortical feed-forward networks for binding different streams of sensory information. Nat Neurosci. 2006;9:1472–3.

Katona G, Szalay G, Maák P, Kaszás A, Veress M, Hillier D, et al. Fast two-photon in vivo imaging with three-dimensional random-access scanning in large tissue volumes. Nat Methods. 2012;9:201–8.

Kazama H, Wilson RI. Origins of correlated activity in an olfactory circuit. Nat Neurosci. 2009;12:1136–44.

Kettunen P, Demas J, Lohmann C, Kasthuri N, Gong Y, Wong ROL, et al. Imaging calcium dynamics in the nervous system by means of ballistic delivery of indicators. J Neurosci Methods. 2002;119:37–43.

Knöpfel T. Genetically encoded optical indicators for the analysis of neuronal circuits. Nat Rev Neurosci. 2012;13:687–700.

Kurebayashi N, Harkins AB, Baylor SM. Use of fura red as an intracellular calcium

indicator in frog skeletal muscle fibers. Biophys J. 1993;64:1934–60.

Linsenbardt AJ, Chisari M, Yu A, Shu H-J, Zorumski CF, Mennerick S. Noncompetitive, voltage-dependent NMDA receptor antagonism by hydrophobic anions. Mol Pharmacol. 2013;83:354–66.

Markram H, Lübke J, Frotscher M, Roth A, Sakmann B. Physiology and anatomy of synaptic connections between thick tufted pyramidal neurones in the developing rat neocortex. J Physiol. 1997;500:409–40.

Mason A, Nicoll A, Stratford K. Synaptic transmission between individual pyramidal neurons of the rat visual cortex *in vitro*. J Neurosci. 1991;11:72–84.

Neunlist M, Peters S, Schemann M. Multisite optical recording of excitability in the enteric nervous system. Neurogastroenterol Motil. 1999;11:393-402.

Obaid AL, Koyano T, Lindstrom J, Sakai T, Salzberg BM. Spatiotemporal patterns of activity in an intact mammalian network with single-cell resolution: Optical studies of nicotinic activity in an enteric plexus. J Neurosci. 1999;19:3073–93.

O'Brien JA, Lummis SCR. Diolistic labeling of neuronal cultures and intact tissue using a hand-held gene gun. Nat Protoc. 2006;1:1517–21.

Otsuka T, Kawaguchi Y. Firing-pattern-dependent specificity of cortical excitatory feed-forward subnetworks. J Neurosci. 2008;28:11186–95.

Pagès S, Côté D, De Koninck P. Optophysiological approach to resolve neuronal action potentials with high spatial and temporal resolution in cultured neurons. Front Cell Neurosci. 2011;5:20.

Perkel DH, Gerstein GL, Moore GP. Neuronal spike trains and stochastic point processes. II. Simultaneous spike trains. Biophys J. 1967;7:419–40.

Pongs O. Voltage-gated potassium channels: from hyperexcitability to excitement. FEBS Lett. 1999;452:31–5.

Prentice JS, Homann J, Simmons KD, Tkačik G, Balasubramanian V, Nelson PC. Fast, scalable, Bayesian spike identification for multi-electrode arrays. PLoS One. 2011;6:e19884.

Reddy GD, Saggau P. Fast three-dimensional laser scanning scheme using acousto-optic deflectors. J Biomed Opt. 2005;10:064038.

Ross WN. Understanding calcium waves and sparks in central neurons. Nat Rev Neurosci. 2012;13:157–68.

Salome R, Kremer Y, Dieudonne S, Leger J-F, Krichevsky O, Wyart C, et al. Ultrafast random-access scanning in two-photon microscopy using acousto-optic deflectors. J Neurosci Methods. 2006;154:161–74.

Schwindel CD, Ali K, McNaughton BL, Tatsuno M. Long-term recordings improve the detection of weak excitatory-excitatory connections in rat prefrontal cortex. J

Neurosci. 2014;34:5454–67.

Segev R, Goodhouse J, Puchalla J, Berry MJ. Recording spikes from a large fraction of the ganglion cells in a retinal patch. Nat Neurosci. 2004;7:1154–61.

Simms BA, Zamponi GW. Neuronal voltage-gated calcium channels: structure, function, and dysfunction. Neuron. 2014;82:24–45.

Sjulson L, Miesenböck G. Rational optimization and imaging in vivo of a genetically encoded optical voltage reporter. J Neurosci. 2008;28:5582–93.

Song S, Sjöström PJ, Reigl M, Nelson S, Chklovskii DB. Highly nonrandom features of synaptic connectivity in local cortical circuits. PLoS Biol. 2005;3:e68.

Sporns O. Networks of the Brain. The MIT Press; 2010.

Stetter O, Battaglia D, Soriano J, Geisel T. Model-free reconstruction of excitatory neuronal connectivity from calcium imaging signals. PLoS Comput Biol. 2012;8:e1002653.

Storace DA, Braubach OR, Jin L, Cohen LB, Sung U. Monitoring brain activity with protein voltage and calcium sensors. Sci Rep. 2015;5:10212.

Takahashi N, Sasaki T, Matsumoto W, Matsuki N, Ikegaya Y. Circuit topology for synchronizing neurons in spontaneously active networks. Proc Natl Acad Sci U S A. 2010;107:10244–9.

Takahashi S, Anzai Y, Sakurai Y. A new approach to spike sorting for multi-neuronal activities recorded with a tetrode--how ICA can be practical. Neurosci Res. 2003;46:265–72.

Tancredi V, Avoli M. Control of spontaneous epileptiform discharges by extracellular potassium: an “in vitro” study in the CA1 subfield of the hippocampal slice. Exp Brain Res. 1987;67:363–72.

Thomson AM, Deuchars J. Synaptic interactions in neocortical local circuits: dual intracellular recordings in vitro. Cereb Cortex. 1997;7:510–22.

Thomson AM, West DC, Wang Y, Bannister AP. Synaptic connections and small circuits involving excitatory and inhibitory neurons in layers 2-5 of adult rat and cat neocortex: triple intracellular recordings and biocytin labelling in vitro. Cereb Cortex. 2002;12:936–53.

Vennekens R, Menigoz A, Nilius B. TRPs in the Brain. Rev Physiol Biochem Pharmacol. 2012;163:27–64.

Vigneron V, Chen H. Sparse data analysis strategy for neural spike classification. Comput Intell Neurosci. 2014;2014:e757068.

Vogt KE, Gerharz S, Graham J, Canepari M. High-resolution simultaneous voltage and $Ca^{2+}$ imaging. J Physiol. 2011;589:489–94.

Wiegner AW, Wierzbicka MM. A method for assessing significance of peaks in

cross-correlation histograms. J Neurosci Methods. 1987;22:125–31.

Wu JY, Cohen LB, Falk CX. Neuronal activity during different behaviors in Aplysia: a distributed organization. Science. 1994;263:820–3.

Yan P, Acker CD, Zhou W-L, Lee P, Bollensdorff C, Negrean A, et al. Palette of fluorinated voltage-sensitive hemicyanine dyes. Proc Natl Acad Sci U S A. 2012;109:20443–8.

Yoshimura Y, Dantzker JLM, Callaway EM. Excitatory cortical neurons form fine-scale functional networks. Nature. 2005;433:868–73.

## 7. Figure Legends

**Figure 1.** Multi-point optical responses of DiO/DPA hybrid voltage-sensitive dye in neurons.

**(A)** Fluorescence image of rat hippocampal neurons at DIV 15 stained with DiO and DPA. Each cross indicates the recorded point with a color matching the trace below. Scale bar: 10 μm. **(B)** Electrophysiological recording (bottom trace) from a single neuron combined with optical recording from neurons at 8 kHz (top traces). Action potentials were evoked in the patch-clamped neuron with a depolarizing step current pulse (400 pA, horizontal bar) for 50 ms under the current clamp mode. A downward deflection of VSD signal indicates depolarization of the membrane potential.

**Figure 2.** Effect of DPA on action potentials in hippocampal neurons.

**(A)** Changes in action potential shape during DPA incubation. Action potentials were evoked by rectangular current pulses in the current-clamp mode of a whole-cell patch-clamp configuration. The kinetics of action potential were slowed and the amplitude was lowered by DPA. Traces were taken before and 1, 5, 10, 15, and 20 min after DPA application. **(B)** The time-course of the half-width of action potential before and after DPA application taken from eight cells, showing an increasing width of action potential in a time-dependent manner. **(C)** The time-course of inhibition of bursting action potential induced with 100 μM 4AP in a hippocampal cultured neuron at DIV13. **($C_1$)** Bursting of spikes started 1 min after exposure to 4AP. **($C_2$)** The spiking gradually decreased by 8 min after exposure to 4AP and DPA (2 μM). **($C_3$)** Spiking completely diminished by 16 min after exposure to 4AP and DPA. **($C_4$)** Spiking recovered by 1.5 min after washing out DPA with ACSF and 4AP. **(D)** Comparison of conditions for evoking action potentials in cultured neurons. Latency of spontaneous action potentials after changing to stimulating bath solutions with DPA, duration of spiking in the stimulating bath solution with DPA, and wash-out latency of DPA with stimulating solutions. Seven μM picrotoxin in ACSF (n = 5), $Mg^{2+}$-free ACSF (n = 4), high $K^+$ (3.8 and 5.5 mM, n = 5 and 4, respectively), ACSF ,and ACSF + 4AP (50 and 100 μM, n =

5 and 4, respectively) were used as stimulating solutions.

**Figure 3.** Electrophysiological and optical recordings of action potentials.
**(A)** A rat hippocampal neuron at DIV 20 was stained with DiO/DPA. Scale bar: 10 μm. The red cross indicates the optical recording point. Scale bar: 10 μm. **(B)** DiO/DPA optical (upper trace) and electrical (lower trace) recordings show action potentials induced by 4AP (50 μM). The optical recording was sampled at 2 kHz and displayed after low-pass filtering with a 9-point moving average filter. **(C)** A part of panel B (horizontal bar) is expanded. The optical trace is not filtered. **(D)** Superimposed 46 spike events. Optical (top) and electrophysiological (bottom) traces of spike events without filter are superimposed (gray traces). Optical records were temporally adjusted by the peak time of corresponding electrical records. Blue and black traces show raw data of single spike (first spike without filter) and average of 46 spike events (blue traces), respectively.

**Figure 4.** Simultaneous voltage and calcium imaging of neuron firing.
Hippocampal cultured neurons (DIV14 (**A**) and DIV22 (**B**)) were stained with Asante Calcium Red and DiO/DPA, and spikes were evoked with 100 μM 4AP. VSD and calcium signals were recorded at 2.5 kHz from eight locations **(A)** and at 1.4 kHz from 14 locations **(B)**. Traces are shown after a low-pass filter was applied (Butterworth, 50 and 10 Hz for voltage and Ca traces, respectively). Upward deflection of the Asante Calcium Red signal indicates Ca increase. Shaded areas in panel $\mathbf{B_1}$ were extended in panels $\mathbf{B_2}$ and $\mathbf{B_3}$.

**Figure 5.** Neuron connections and their directions as revealed by cross-correlation analysis.
**(A)** Neuron culture (DIV14) was stained with DiO. Each colored cross indicates a recording point corresponding to the colored trace below. Scale bar: 50 μm. **(B)** Action potentials were evoked with 100 μM 4AP, and membrane potential was optically recorded at 20 points in different neurons at 1.25 kHz. Spike activities were observed in

six cells, fluorescence changes of which are indicated after filtering with a 50 Hz low-pass Butterworth filter. **(C)** Five consecutive 200-sec voltage recordings were performed, and cross-correlation of spike timing for each neuron pair was calculated for each recording. Cross-correlation of five consecutive recordings was accumulated. Black and gray bars represent significant and insignificant connections, respectively, as determined by the Z-test (see Materials and Methods). Note that most bars are colored black. **(D)** Distribution in lag of spike events between each neuron pair was calculated. Neuron pairs judged as asymmetrical spike lag distribution, *i.e.*, unidirectional connection, showed 4.8 ± 0.5 ms lag (n = 57, blue histogram). Lag distribution of neuron pairs judged as symmetrical lag distribution are shown as a dotted histogram.

Figure 1, Shafeghat et al. (single column width)

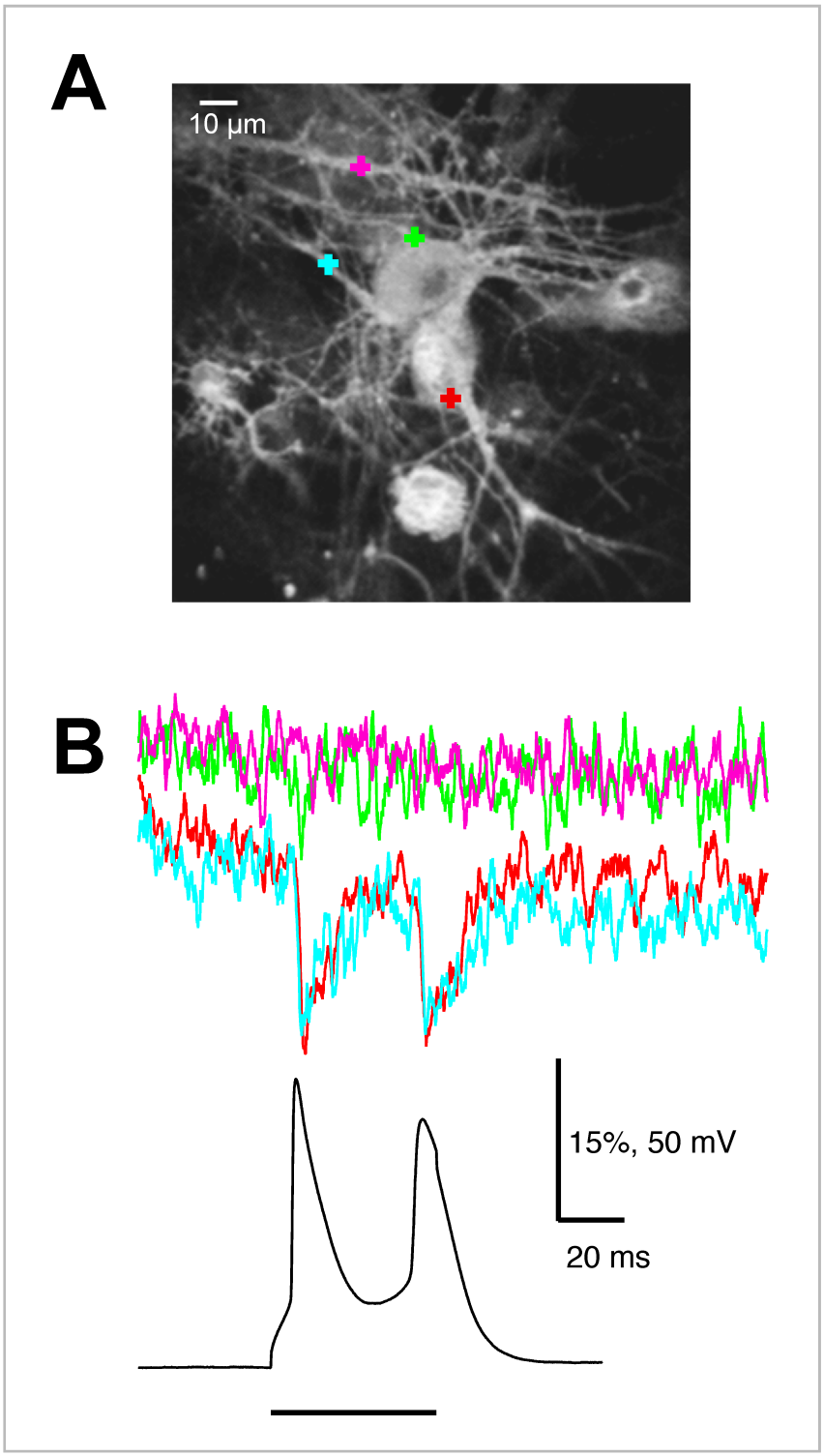

Figure 2, Shafeghat et al. (single column width)

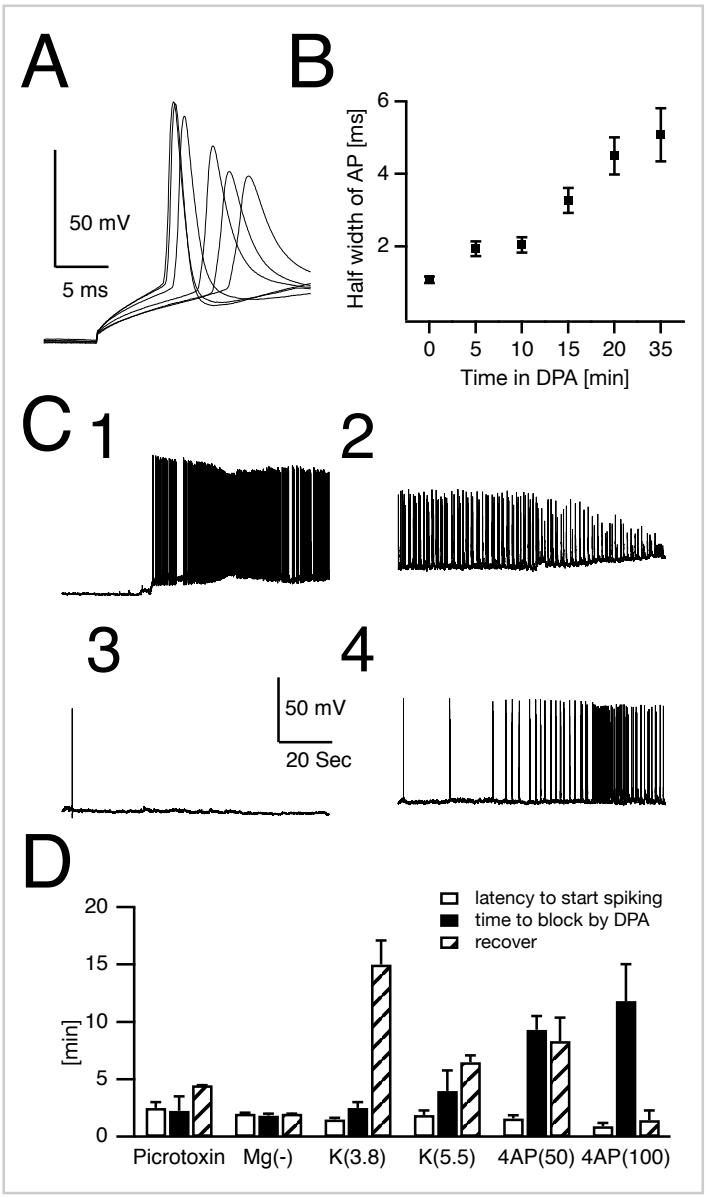

Figure 3, Shafeghat et al. (1.5 column width)

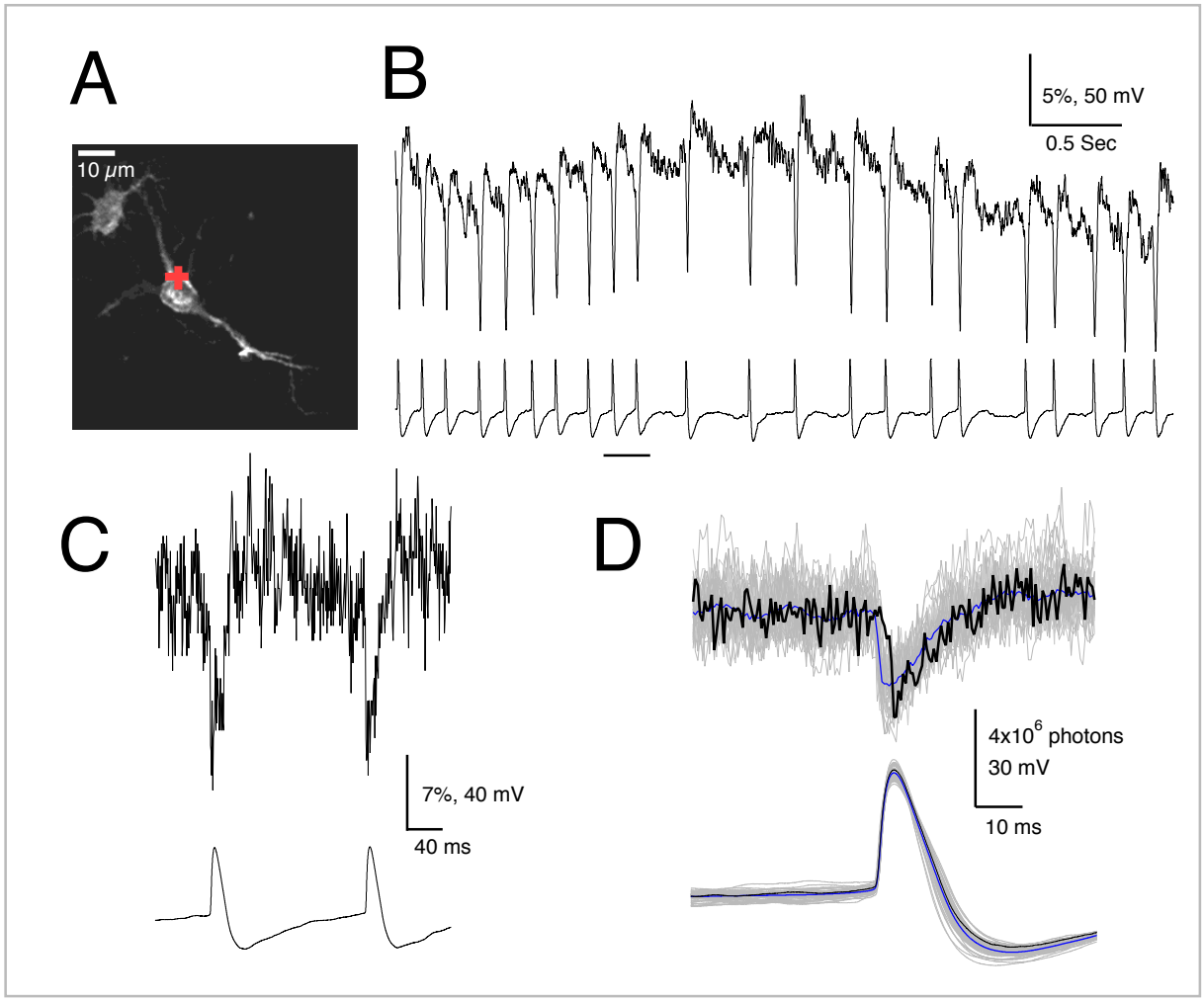

Figure 4, Shafeghat et al. (single column width)

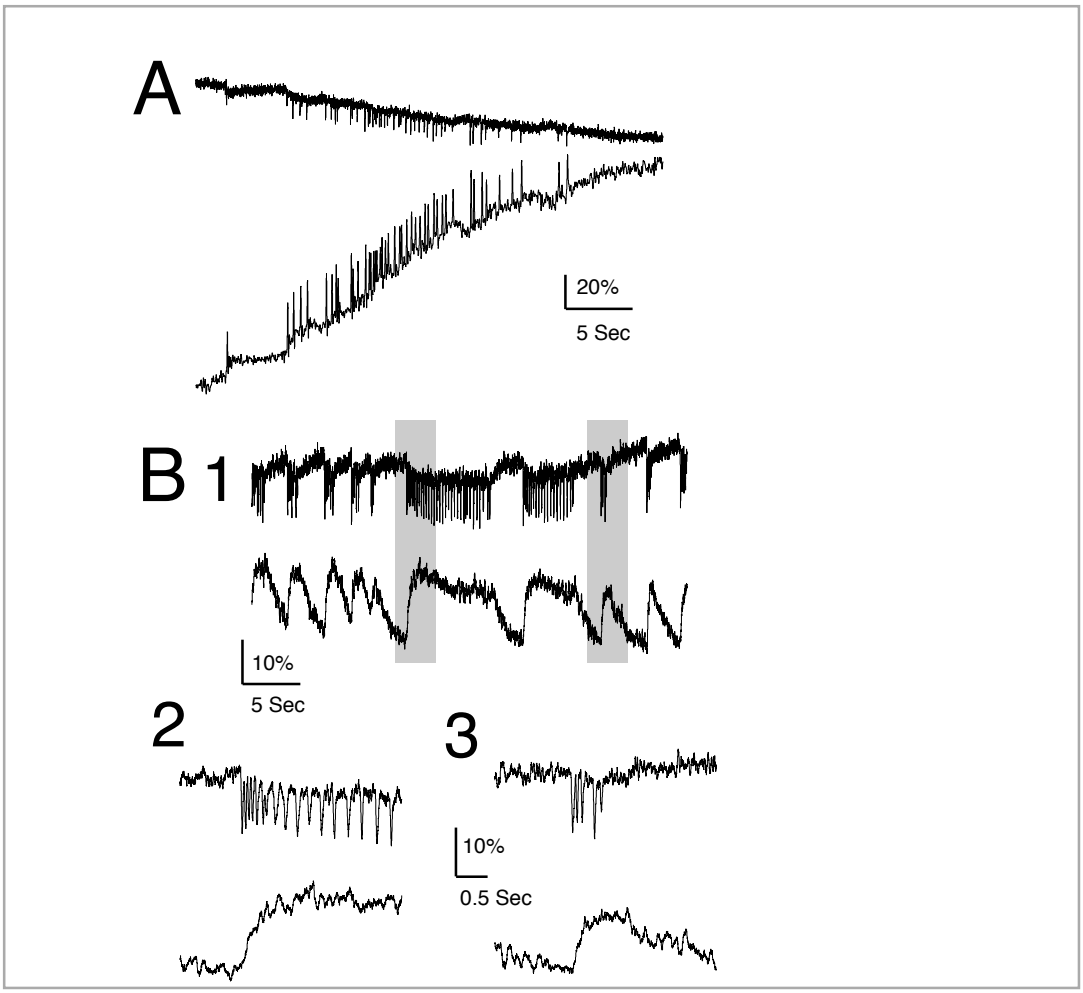

Figure 5, Shafeghat et al. (1.5 column width)